Supplementary Material
Twin-focus photothermal correlation spectroscopy

Markus Selmke, Romy Schachoff, Marco Braun, and Frank Cichos

November 14, 2012

1 Materials & Methods

All measurements have been carried out in an inverted home-built photothermal microscopy setup in forward detection configuration. The setups consists of a heating ($\lambda_h = 532\,\mathrm{nm}$, Coherent Verdi) and a probe laser ($\lambda_d = 635\,\mathrm{nm}$, Coherent ULN laser diode) both focused into the sample plane by a 100x/NA1.4 microscope objective lens (Olympus). The probe light is collected by a second microscope objective (Olympus, 50x/NA 0.8) and imaged to a photodiode (Thorlabs, PDA36A-EC) recording the transmitted detection laser power P_d. The photodiode signal is analyzed by a lock-in amplifier (Signal Recovery 7280 DSP) to filter out the probe beam modulation on the frequency of the heating laser modulation at $\Omega = 300\,\mathrm{kHz}$. The X and Y channels of the lock-in amplifier are digitized by an ADC (Jäger AdWin Gold). The phase-sensitive experimental photothermal signal $\tilde{\Phi}$ is gained as follows:

$$\tilde{\Phi} = \frac{\Delta P_d}{P_d} = \cos(\phi - \phi_{\mathrm{LI}})\sqrt{X^2+Y^2}, \quad \tan\phi = X/Y. \tag{1}$$

Here, ϕ_{LI} is an artificial phase angle that can be set at the lock-in amplifier. To calibrate the setup scattering images of immobilized gold nanoparticles (AuNPs) with a radius of $R = 30$ nm are taken at the excitation and detection wavelength, respectively. The overlap of these two images was confirmed or, if necessary, adjusted. Then z-scans of the photothermal signal were taken and fitted with the functional analytical approximation Φ to the photothermal signal

$$\Phi(\mathbf{r}) = \Phi(z,\rho) = \Phi_0 \exp\left(-\frac{2\rho^2}{\omega_\rho^2}\right)[z_0 - z]\exp\left(-\frac{2z^2}{\omega_z^2}\right) \tag{2}$$

to gain the lateral and axial parameters ω_ρ and ω_z and the asymmetry parameter z_0. This signal-form is composed of a positive and a negative half according to $\Phi = \Phi_+ + \Phi_-$ with $\Phi_-(\mathbf{r}) = \Phi(z,\rho)\,\Theta(z - z_0)$ and $\Phi_+(\mathbf{r}) = \Phi(z,\rho)\,\Theta(z_0 - z)$ in which $\Theta(z)$ denotes the Heavyside function.

For the diffusion measurements the symmetric configuration of the photothermal signal ($z_0 = 0$) was chosen. The sample in the photothermal correlation experiments was an aqueous solution of AuNPs of $R = 14\,\mathrm{nm}$, confined between two cover-slides. In addition, the sample cell was sealed using polydimethylsiloxane (Sylgard 184) to avoid an evaporation of the solvent. Photothermal signal time-traces were recorded at an acquisition rate of 50 kHz what corresponds to a time resolution of $20\,\mu\mathrm{s}$. While every recorded event contributes to the ACF, events that contribute to the CCF are less often. To ensure reasonable statistics, the length of each time-trace is at least 1 h at a particle concentration of $2.6 \cdot 10^{10}\,\mathrm{ml}^{-1}$. Both lock-in channels X and Y were analyzed by their histograms and a possible DC-offset (AdWin) in the signal has to be corrected. The phase-sensitive signal was calculated using Eq. 1. To achieve the symmetric signal calibration scenario and a signal described by Eqn. 2 with $z_0 = 0$, the phase-sensitive photothermal signal histograms have been checked again to be symmetric about the origin.

1.1 Data processing

For a discrete time-trace of N values $\tilde{\Phi}_i$ was recorded in time-steps of Δt, i.e. $\tilde{\Phi}_i = \tilde{\Phi}(i\Delta t)$, we compute the correlation functions from the experimental time traces via

$$G_{\mathrm{ACF}}\left(j\Delta t\right) = \frac{\frac{1}{N}\sum_i^N \tilde{\Phi}_i \tilde{\Phi}_{i+j}}{\left[\frac{1}{N}\sum_i^N \left|\tilde{\Phi}_i\right|\right]^2} - 1 \tag{3}$$

The histograms $N\left(\tilde{\Phi}\right)$ of the phase-sensitive signal traces have been fitted with a gaussian peak $\mathcal{N}\left(\mu_\Phi, \sigma^2\right)$ with variance σ^2 and possibly non-zero mean μ_Φ. They have been shifted by μ_S to ensure zero-centered noise. The phase-sensitive ACF $G_{\mathrm{ACF}}^{\mathrm{ps}}$ was then computed right-away according to Eqn. 3. For the magnitude auto-correlation function $G_{\mathrm{ACF}}^{\mathrm{abs}}$ the absolute value of the phase-sensitive trace has been shifted by the mean of the thereby one-sided gaussian noise:

$$\langle\left|\mathcal{N}\left(0,\sigma^2\right)\right|\rangle = [2/\pi]^{1/2}\,\sigma, \tag{4}$$

i.e. by $\left|\tilde{\Phi}_i\right| \rightarrow \left|\tilde{\Phi}_i\right| - [2/\pi]^{1/2}\,\sigma$. This shifts the signal as well, and gives a reduced contrast as compared to the correct value of phase-sensitive ACF, $G_{\mathrm{ACF}}(0)$, i.e. $G_{\mathrm{ACF}}^{\mathrm{abs}}(0) < G_{\mathrm{ACF}}^{\mathrm{abs}}(0)$, and a decay to zero. For the computation of the single lobe auto-correlation functions G_{ACF}^{+} and G_{ACF}^{-} and the cross-correlation functions G_{CCF}^{+-} and G_{CCF}^{-+} we have split the phase-sensitive signal-trace further into $\tilde{\Phi}_i^{+}$ and $\tilde{\Phi}_i^{-}$ according to the following rule:

$$\tilde{\Phi}_i^{\pm} = \begin{cases} \tilde{\Phi}_i & \text{if } \tilde{\Phi}_i \gtrless 0, \\ \pm\left|\mathcal{N}(0,\sigma^2)\right| & \text{if } \tilde{\Phi}_i \lesseqgtr 0. \end{cases} \tag{5}$$

White gaussian noise $\mathcal{N}(0,\sigma^2)$ of zero mean and variance σ^2 with matching sign was written into each trace: Whenever there is positive signal written into $\tilde{\Phi}^{+}$, negative noise is added to $\tilde{\Phi}^{-}$, and vice versa. Thereby, each channel consists of positive or negative values only. These individual traces have been shifted by $\pm[2/\pi]^{1/2}\,\sigma$ as well to ensure a total noise, that is the artificially added and the signal-contained noise, with zero mean. In case of the single lobe ACFs, the denominator in Eqn. 3 was replaced by the self-normalization $\left[\frac{1}{N}\sum_i^N \tilde{\Phi}_i^{\pm}\right]^2$. For the cross-correlation, the signed timetrace $\tilde{\Phi}^{+}$ is correlated with $\tilde{\Phi}^{-}$, and vice versa. All cross- and auto-correlation functions decay to zero, and the cross-correlation functions obtained in this way start at zero, too. In case of the single lobe ACFs, the denominator in Eqn. 3 was replaced by the self-normalization $\left[\frac{1}{N}\sum_i^N \tilde{\Phi}_i^{\pm}\right]^2$.

The normalization of a noise-mean shifted signal which contains noise is approximately equal to the mean of the signal itself, e.g. the correct normalization considered in the theory:

$$\langle\left|\tilde{\Phi}^{\mathcal{N}}\right|_{\mathrm{shifted}}\rangle = \langle\left|\tilde{\Phi} + \mathcal{N}\left(0,\sigma^2\right)\right| - [2/\pi]^{1/2}\,\sigma\rangle = \langle\left|\tilde{\Phi} + \mathcal{N}\left(0,\sigma^2\right)\right|\rangle - [2/\pi]^{1/2}\,\sigma \lessapprox \langle\left|\tilde{\Phi}\right|\rangle + \langle\left|\mathcal{N}\left(0,\sigma^2\right)\right|\rangle - [2/\pi]^{1/2}\,\sigma = \langle\left|\tilde{\Phi}\right|\rangle$$

2 Correlation Functions

2.1 Diffusion Propagator and Analytical Formulation

In order to obtain the theoretical (cross-)correlation function for brownian particles, the following 6-fold integral needs to be computed:

$$G(\tau) = \frac{\int\int \Phi_a(\mathbf{r})\,\Phi_b(\mathbf{r}')\,p(\tau,\mathbf{r},\mathbf{r}')\,\mathrm{d}\mathbf{r}\,\mathrm{d}\mathbf{r}'}{\langle C\rangle\left(\int |\Phi(\mathbf{r})|\,\mathrm{d}\mathbf{r}\right)^2} \tag{6}$$

Here, Φ_a and Φ_b depend on the type of correlation function considered, see table 1. The diffusion process in the presence of an additional deterministic flow $\mathbf{V}(\mathbf{r})$ is described by the advection diffusion equation (ADE): $\partial C/\partial t = D\nabla^2 C - \nabla\cdot(\mathbf{V}C)$. Herein, D is the diffusion coefficient of the Brownian particles. The ADE is solved using the advection-diffusion propagator $p(\tau,\mathbf{r},\mathbf{r}')$, i.e. the Green's function of the ADE [**?**]:

$$p\left(\tau,\mathbf{r},\mathbf{r}'\right) = \frac{\exp\left(-|\mathbf{r}-\mathbf{r}'+\mathbf{V}\tau|^2/[4D\tau]\right)}{(4\pi D\tau)^{3/2}}. \tag{7}$$

It includes three terms in the argument of the exponential function. One is the squared distance between the position vectors $\mathbf{r}$ and $\mathbf{r}'$, the second is the scalar product of this distance vector with the flow velocity vector $\mathbf{V}$, and the last term contains the squared velocity vector. In cylindrical coordinates $\{\rho,\phi,z\}$ the distance squared may be written as $|\mathbf{r}-\mathbf{r}'|^2 = (z-z')^2 + \rho^2 + \rho'^2 - 2\rho\rho'\cos\left(\phi-\phi'\right)$. This term is the only term in the free diffusion propagator. If flow is present, and an axial flow

is considered only such that $\mathbf{V} = V_z\hat{\mathbf{z}}$, the two other terms amount to a factor of $\exp\left(-V_z^2\tau/4D\right)\exp(-2V_z(z-z')/4D)$. The integrals with respect to the polar angles ϕ and ϕ' and the radial coordinates ρ and ρ' constitute a reoccuring part of the integrals. This leaves only the z and z' integrations left to be done for the various correlation functions.

For lateral flow, cartesian coordinates were used and the advection-diffusion propagator:

$$p\left(\tau,\mathbf{r},\mathbf{r}'\right) = \frac{\exp\left(-\left[(x-x'+V_x\tau)^2+(y-y')^2+(z-z'+V_z\tau)^2\right]/[4D\tau]\right)}{(4\pi D\tau)^{3/2}}. \tag{8}$$

Table 1: Overview of various correlation functions computable from the photothermal signal time-traces. Eqn. 6 was then used to obtain analytical expressions, where $\tilde{\Phi}_a$ and $\tilde{\Phi}_b$ were substituted with the corresponding signal given in the first column. Given are the symbols used in the text without the optional V_z, V_x and z_0 superscripts. Also indicated are the event types the various correlation functions are sensitive to.

signal	corr. type	symbol	event type	section
P_d	ACF	G_{ACF}^{3DG}	③,④	2.3
$\tilde{\Phi}$	ACF	G_{ACF}	③,④	2.5
$\left\|\tilde{\Phi}\right\|$	ACF	$G_{\mathrm{ACF}}^{\mathrm{abs}}$	③,④	2.7
$\tilde{\Phi}_+$	ACF	G_{ACF}^{+}	④	2.8
$\tilde{\Phi}_-$	ACF	G_{ACF}^{-}	③	2.8
$\left\{\tilde{\Phi}_+,\tilde{\Phi}_-\right\}$	CCF	G_{CCF}^{+-}	②	2.6
$\left\{\tilde{\Phi}_-,\tilde{\Phi}_+\right\}$	CCF	G_{CCF}^{-+}	①	2.6

Table 2: Overview of various introduced abbreviations which appear in the analytical or numerical expressions of the presented correlation functions

symbol	expression
τ_D	$\omega_\rho^2/(4D)$
γ	ω_z/ω_ρ
Γ_1	$\left[1+\frac{\tau}{\tau_D}\right]$
Γ_2	$\left[\gamma^2+\frac{\tau}{\tau_D}\right]$
Γ_3	$\left[\gamma^2+2\frac{\tau}{\tau_D}\right]$
Z	$\sqrt{2}z_0/\left(\gamma\omega_\rho\right)$
a	$b/2+2/\left(\gamma^2\omega_\rho^2\right)$
b	$2\frac{\tau_D}{\tau}/\omega_\rho^2$
f	$2V_z\tau_D/\omega_\rho^2$
K	$\left[bz'-f-2az_0\right]/\left(2\sqrt{a}\right)$
H	$\left(bz'-f\right)/\left(2\sqrt{a}\right)$

2.2 Common factor to all considered correlation functions

The integrals with respect to the polar angles ϕ and ϕ' and the radial coordinates ρ and ρ' constitute a reoccuring part of the integrals common to all evaluated correlation functions and yield

$$\frac{1}{\langle C\rangle(4\pi D\tau)^{3/2}}\int_{\phi,\phi'=0}^{2\pi}\int_{\rho,\rho'=0}^{\infty}p_{\rho,\phi}\left(\rho,\rho',\phi,\phi'\right)\exp\left(-\frac{2\left[\rho^2+\rho'^2\right]}{\omega_\rho^2}\right)\mathrm{d}\phi\,\mathrm{d}\phi'\rho\,\mathrm{d}\rho\,\rho'\mathrm{d}\rho' = \frac{\omega_\rho\pi^{1/2}}{4\langle C\rangle\left(1+\frac{\tau}{\tau_D}\right)\left(\frac{\tau}{\tau_D}\right)^{1/2}} \tag{9}$$

where $p_{\rho,\phi} = \exp\left(-\left[\rho^2+\rho'^2-2\rho\rho'\cos\left(\phi-\phi'\right)\right]/4D\tau\right)$ is the factor of the diffusion propagator which depends on these coordinates. The exponential factor stems from the signal function being a gaussian in lateral direction for both FCS and Twin-PhoCS.

2.3 Regular FCS, i.e. 3D gaussian detection volume

In standard FCS, an azimuthally symmetric 3D-gaussian focus geometry is assumed, i.e. the detected fluorescence signal is assumed to be $P_d(\mathbf{r}) = P_0 \exp\left(-2\rho^2/\omega_\rho^2\right)\exp\left(-2z^2/\omega_z^2\right)$, with a lateral and axial beam-waist of ω_ρ and $\omega_z = \gamma\omega_\rho$, respectively, and one finds for the case of axial flow and lateral flow, i.e. for $\mathbf{V} = V_x\hat{\mathbf{x}} + V_z\hat{\mathbf{z}}$:

$$G_{\mathrm{ACF}}^{3DG,V_x,V_z}(\tau) = \exp\left(-\frac{V_x^2\tau^2}{\omega_\rho^2\Gamma_1}\right)\exp\left(-\frac{V_z^2\tau^2}{\omega_\rho^2\Gamma_2}\right)\frac{\gamma}{\langle N\rangle\Gamma_1\Gamma_2^{1/2}}, \tag{10}$$

where the effective particle number density in the focus is $\langle N\rangle = \langle C\rangle V_{\mathrm{eff}}^{3DG}$. Note that some authors write $\left[1+\gamma^{-2}\frac{\tau}{\tau_D}\right]$ instead of Γ_2, thus missing the factor of γ which is present here. The effective focal volume for a 3D-Gaussian is given by

$$V_{\mathrm{eff}}^{3DG} = \left[\int |P_d(\mathbf{r})|\,\mathrm{d}\mathbf{r}\right]^2 \Big/ \int |P_d(\mathbf{r})|^2\,\mathrm{d}\mathbf{r} = \pi^{3/2}\gamma\omega_\rho^3. \tag{11}$$

The contrast of the FCS correlation function is the inverse of the mean particle number within the effective focal volume, i.e. $G_{\mathrm{ACF}}^{3DG,V_x,V_z}(0) = 1/\langle N\rangle$ with $\langle N\rangle = \langle C\rangle V_{\mathrm{eff}}^{3DG}$.

2.4 Common normalization in Twin-PhoCS

The normalization, i.e. the denominator in Eqn. 6, for the case of a twin-focus photothermal detection volume reads:

$$\left(\int |\Phi(\mathbf{r})|\,\mathrm{d}\mathbf{r}\right)^2 = \left[\int_0^{2\pi}\mathrm{d}\phi\int_{-\infty}^{\infty}\mathrm{d}z\int_0^{\infty}\rho\,\mathrm{d}\rho\,\Phi_0\,|z_0-z|\exp\left(\frac{-2z^2}{\omega_z^2}\right)\exp\left(\frac{-2\rho^2}{\omega_\rho^2}\right)\right]^2 \tag{12}$$

$$= \Phi_0^2\left[\frac{\pi}{4}\gamma^2\omega_\rho^4\right]^2 \times \left\{\exp\left(-2Z^2\right)\left[1+Z\exp\left(Z^2\right)\sqrt{\pi}\,\mathrm{Erf}(Z)\right]^2\right\} \approx \Phi_0^2\left[\frac{\pi}{4}\gamma^2\omega_\rho^4\right]^2 \times \left[1+2Z^2+\mathcal{O}\left(Z^4\right)\right], \tag{13}$$

where $\mathrm{Erf}(x) = 2\pi^{-1/2}\int_0^x \exp(-t^2)\,\mathrm{d}t$ is the error-function and the expansion is for $Z \ll 1$.
The effective focal volume defined as above (Eqn. 11) now with the PT signal function evaluates to:

$$V_{\mathrm{eff}}^{z_0} = 4\sqrt{\pi}\gamma\,\omega_\rho^3 \times \left\{\frac{\exp(-2Z^2)\left[1+\sqrt{\pi}Z\exp(Z^2)\,\mathrm{Erf}(Z)\right]^2}{4Z^2+1}\right\} \quad \begin{array}{l} \approx 4\sqrt{\pi}\gamma\,\omega_\rho^3 \times [1-2Z^2+\mathcal{O}(Z^4)] \\ \to 4\sqrt{\pi}\gamma\,\omega_\rho^3 \times \frac{\pi}{4} \end{array}. \tag{14}$$

The limit corresponds to $Z \to \pm\infty$. The above expressions simplify for the symmetric configuration of the twin-focal volume, i.e. for $z_0 = Z = 0$ the term in the curly brackets becomes $\{\ldots\} = 1$. The symmetric ($Z = 0$) twin-focal volume is simply $V_{\mathrm{eff}} = 4\sqrt{\pi}\gamma\,\omega_\rho^3$.

2.5 Phase sensitive auto-correlation function, G_{ACF}

For the phase-sensitve signal the autocorrelation function in the most general situation of an asymmetric twin focus with axial and lateral flow, i.e. $\mathbf{V} = V_x\hat{\mathbf{x}} + V_z\hat{\mathbf{z}}$, one finds explicitely:

$$G_{\mathrm{ACF}}^{V_x,V_z,z_0} = \exp\left(\frac{-V_x^2\tau^2}{\Gamma_1\,\omega_\rho^2}\right)\exp\left(-\frac{V_z^2\tau^2}{\Gamma_2\omega_\rho^2}\right)\frac{1}{4\langle C\rangle\sqrt{\pi}\Gamma_1\Gamma_2^{3/2}\omega_\rho^3}\left\{\frac{\exp(2Z^2)\left[4Z^2\Gamma_2+\gamma^2\left(1-2\frac{V_z^2\tau^2}{\Gamma_2\omega_\rho^2}\right)\right]}{\left[1+\sqrt{\pi}Z\exp\left(Z^2\right)\mathrm{Erf}(Z)\right]^2}\right\}, \tag{15}$$

$$G_{\mathrm{ACF}}^{V_x,V_z}(\tau) = G_{\mathrm{ACF}}(\tau)\times\exp\left(\frac{-V_x^2\tau^2}{\Gamma_1\,\omega_\rho^2}\right)\exp\left(\frac{-V_z^2\tau^2}{\Gamma_2\,\omega_\rho^2}\right)\left[1-\frac{2V_z^2\tau^2}{\Gamma_2\,\omega_\rho^2}\right], \tag{16}$$

$$G_{\mathrm{ACF}}(\tau) = \frac{\gamma^3}{\langle N\rangle\Gamma_1\Gamma_2^{3/2}}. \tag{17}$$

The simpler cases of a symmetric twin-focal volume correlation function ($z_0 = 0$, Eqn. 16) and its corresponding form when no flow is present ($V_z = 0$, Eqn. 17) have already been presented in the main article. The term in the curly brackets becomes $\{\ldots\} = \frac{4}{\pi}\Gamma_2$ when $Z \to \pm\infty$ while the effective volume becomes $V_{\mathrm{eff}} \to \pi^{3/2}\gamma\omega_\rho^3$ such that the FCS expression, Eqn. 10, is recovered. At zero lag time, i.e. when $\tau = 0$, the term becomes $\{\ldots\} = \gamma^2/V_{\mathrm{eff}}^{z_0}$ such that also here $G_{\mathrm{ACF}}^{V_x,V_z,z_0}(0) = 1/\langle N\rangle$ with $\langle N\rangle = \langle C\rangle V_{\mathrm{eff}}^{z_0}$ holds true.

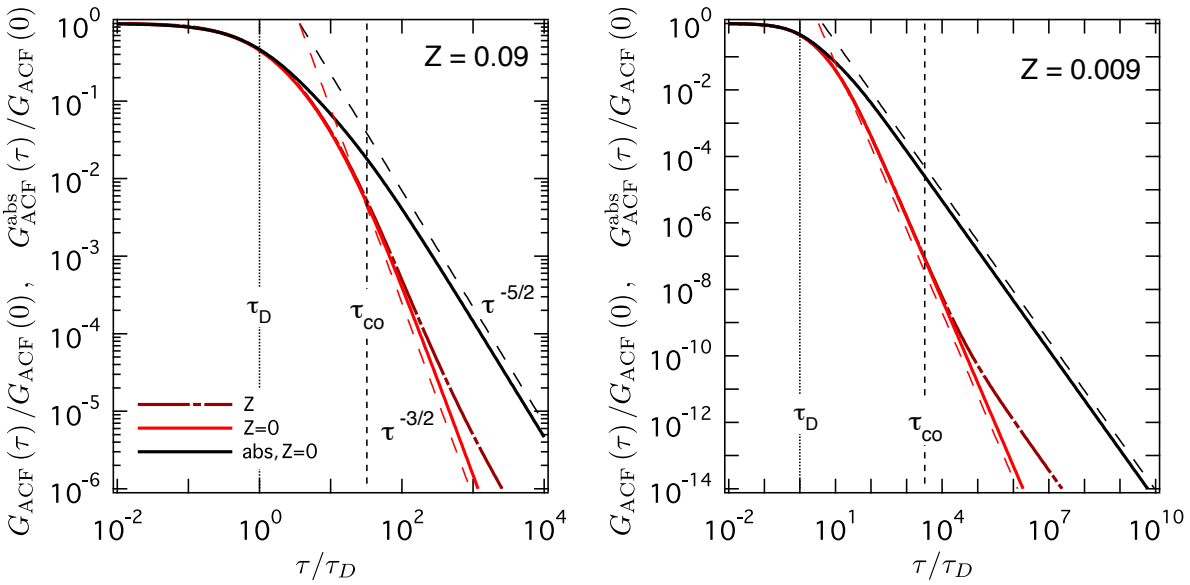

Figure 1: Phase-sensitive ACF and the effect of z_0.

The difference of phase sensitive and absolute value ACF thus has to be negative, which is a direct consequence of the occurring anti-correlating events in the ACF of the phase-sensitive signal. The phase-sensitive ACF decays therefore quicker according to $G_{\rm ACF} \propto (\tau/\tau_D)^{-5/2}$ for the ideal symmetric configuration, while all other functions including the cross-correlation decay according to $G \propto (\tau/\tau_D)^{-3/2}$ at late times $\tau \gg \tau_D$. However, any finite asymmetry in the signal configuration will result in a net-signed detection function leading to a decay of the phase-sensitive ACF with a $-5/2$ power law at intermediate times $\tau_D < \tau < \tau_{\rm co}$ and $-3/2$ at later times $\tau > \tau_{\rm co}$ where the cross-over time is determined by $\tau_{\rm co}/\tau_D = \gamma^2\omega_z^2/\left(8z_0^2\right)$.

2.6 Cross-correlation function, $G_{\rm CCF}^{+-}$

We here consider the cross-correlation $(+ \to -)$ function only with axial flow ($\mathbf{V} = V_z\,\hat{\mathbf{z}}$). Note that the reverse cross-correlation $(- \to +)$ is connected to the expression here by the symmetry relation $G_{\rm CCF}^{-+,V_z,z_0} = G_{\rm CCF}^{+-,-V_z,-z_0}$:

$$G_{\rm CCF}^{+-,V_z,z_0} = \frac{8\left(\frac{\tau}{\tau_D}\right)^{1/2}\exp\left(-\frac{V_z^2\tau^2}{\omega_\rho^2}\frac{\tau_D}{\tau}\right)}{\pi\gamma\,\omega_\rho^2\,\Gamma_1\Gamma_3\left[4Z^2+1\right]}\left[\int_{z_0}^{\infty}\mathrm{d}z'\exp\left(-az'^2\right)\exp\left(z_0\left[bz'-f-az_0\right]\right)\right.$$
$$\left.\times\exp\left(fz'\right)\left[z'-z_0\right]\left\{1-\exp\left(K^2\right)K\sqrt{\pi}\left[1-\mathrm{Erf}(K)\right]\right\}\right], \tag{18}$$

$$G_{\rm CCF}^{+-,V_z} = \frac{-8\sqrt{\frac{\tau}{\tau_D}}\exp\left(-\frac{V_z^2\tau^2}{\omega_\rho^2}\frac{\tau_D}{\tau}\right)}{\langle N\rangle\pi\gamma\,\omega_\rho^2\,\Gamma_1\Gamma_3}\int_0^{\infty}\mathrm{d}z'\exp\left(-az'^2\right)\exp\left(fz'\right)z'\left\{1-\exp\left(H^2\right)H\sqrt{\pi}\left[1-\mathrm{Erf}(H)\right]\right\}, \tag{19}$$

$$G_{\rm CCF}^{+-}(\tau) = \frac{\frac{\gamma^2}{2}\arctan\left(\frac{2}{\gamma^2}\left[\frac{\tau}{\tau_D}\Gamma_2\right]^{1/2}\right)-\left[\frac{\tau}{\tau_D}\Gamma_2\right]^{1/2}}{\langle N\rangle\pi\,\Gamma_1\Gamma_2^{3/2}/\gamma}. \tag{20}$$

To avoid effects due to possibly unstable concentrations in the sample over the period of measurements, it is often convenient to normalize the cross-correlation functions by the contrast of the auto-correlation functions $(1/\langle N\rangle)$. Then, the shape and magnitude of the CCF is only affected by the flow present in the sample. For *small axial flow velocities* the correction to the ACFs is of second order in the velocity while the CCF changes already in first order and is thus intrinsically more sensitive than the ACFs. This will be shown in the following sections:

The propagator for diffusion with flow in the limit of small axial flow velocity $\mathbf{V} = V_z\,\hat{\mathbf{z}}$ reads:

$$p\left(\tau,\mathbf{r},\mathbf{r}',V_z\right) = \frac{1}{(4\pi D\tau)^{3/2}}\exp\left(-\frac{(\mathbf{r}-\mathbf{r}')^2+2\mathbf{V}\cdot(\mathbf{r}-\mathbf{r}')\tau+V^2\tau^2}{4D\tau}\right) \approx \exp\left(-\frac{V_z^2\tau}{4D}\right)\left[1-\frac{2V_z\tau_D}{\omega_\rho^2}\left[z-z'\right]\right]p\left(\tau,\mathbf{r},\mathbf{r}'\right) \tag{21}$$

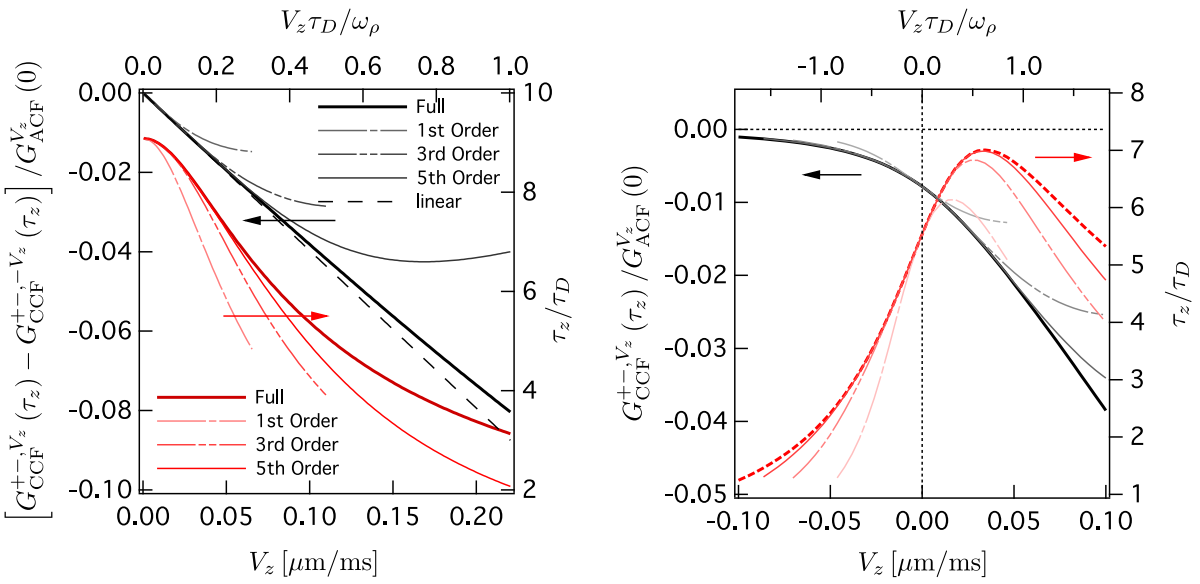

Figure 2: Approximation of the CCF amplitude and CCF difference.

such that to first order, the correlation functions remain the same plus possibly some additional function. As it turns out, the corrective term to the CCF is of first order in the flow velocity, i.e. $\mathcal{O}\left(V_z\tau_D/\omega_\rho\right)$, while the correction to the auto-correlation functions is of smaller second order. The following expressions hold for small enough flow-velocities, i.e. the first, third and fourth order expressions are accurate to within a few percent for $V_z\tau_D/\omega_\rho < 0.1, < 0.3$ and < 0.5, respectively.

$$
\begin{aligned}
G^{+-,V_z}_{\rm CCF} \approx \exp\left(\frac{-V_z^2\tau_D^2}{\omega_\rho^2}\frac{\tau}{\tau_D}\right)\Bigg\{ & G^{+-}_{\rm CCF} \\
& - \left(\frac{V_z\tau_D}{\omega_\rho}\right)\frac{2\gamma^2\left(\frac{\tau}{\tau_D}\right)^2}{\sqrt{\pi}\Gamma_1\Gamma_2^2\Gamma_3^{1/2}} \\
& - \left(\frac{V_z\tau_D}{\omega_\rho}\right)^3\frac{2\gamma^4\left(\frac{\tau}{\tau_D}\right)^3\left[9\frac{\tau}{\tau_D}+5\gamma^2\right]}{3\sqrt{\pi}\Gamma_1\Gamma_2^3\Gamma_3^{3/2}} \\
& - \left(\frac{V_z\tau_D}{\omega_\rho}\right)^2\frac{\frac{\gamma^3}{2}\left(\frac{\tau}{\tau_D}\right)\left[4\left(\frac{\tau}{\tau_D}\right)^2-\gamma^4\right]\arctan\left(\frac{2}{\gamma^2}\sqrt{\frac{\tau}{\tau_D}\Gamma_2}\right)+\left[4\frac{\tau}{\tau_D}+\gamma^2\right]\sqrt{\frac{\tau}{\tau_D}\Gamma_2}}{\pi\Gamma_1\Gamma_2^{5/2}\Gamma_3} \\
& - \left(\frac{V_z\tau_D}{\omega_\rho}\right)^4\frac{\gamma^5\left(\frac{\tau}{\tau_D}\right)^2}{24\pi\Gamma_1\Gamma_2^4\Gamma_3^2}\left[160\left(\frac{\tau}{\tau_D}\right)^{7/2}+48\pi\left(\frac{\tau}{\tau_D}\right)^3\Gamma_2^{1/2}+272\gamma^2\left(\frac{\tau}{\tau_D}\right)^{5/2}+36\pi\gamma^2\left(\frac{\tau}{\tau_D}\right)^2\Gamma_2^{1/2}\right. \\
& \qquad \left.+124\gamma^4\left(\frac{\tau}{\tau_D}\right)^{3/2}+12\gamma^6\left(\frac{\tau}{\tau_D}\right)^{1/2}-3\pi\gamma^6\Gamma_2^{1/2}-6\left(4\frac{\tau}{\tau_D}-\gamma^2\right)\Gamma_2^{1/2}\Gamma_3^2\arctan\left(\frac{\gamma^2}{2}/\sqrt{\frac{\tau}{\tau_D}\Gamma_2}\right)\right] \\
& - \left(\frac{V_z\tau_D}{\omega_\rho}\right)^5\frac{\gamma^6\left(\frac{\tau}{\tau_D}\right)^4\left[115\left(\frac{\tau}{\tau_D}\right)^2+126\gamma^2\left(\frac{\tau}{\tau_D}\right)+35\gamma^4\right]}{15\sqrt{\pi}\Gamma_1\Gamma_2^4\Gamma_3^{5/2}}\Bigg\}
\end{aligned}
\tag{22}
$$

The *difference* of the CCFs to fifth order $\mathcal{O}\left(V_z\tau_D/\omega_\rho\right)^5$ reads:

$$
\begin{aligned}
G^{+-,V_z}_{\rm CCF} - G^{-+,V_z}_{\rm CCF} = G^{+-,-V_z}_{\rm CCF} - G^{+-,+V_z}_{\rm CCF} \approx -\exp\left(\frac{-V_z^2\tau_D^2}{\omega_\rho^2}\frac{\tau}{\tau_D}\right)\frac{4\gamma^2\left(\frac{\tau}{\tau_D}\right)^2}{\sqrt{\pi}\Gamma_1\Gamma_2^2\Gamma_3^{1/2}}\times \\
\left\{\left(\frac{V_z\tau_D}{\omega_\rho}\right)+\left(\frac{V_z\tau_D}{\omega_\rho}\right)^3\frac{\gamma^2}{3\Gamma_3\Gamma_2}\left(\frac{\tau}{\tau_D}\right)\left[9\frac{\tau}{\tau_D}+5\gamma^2\right]+\left(\frac{V_z\tau_D}{\omega_\rho}\right)^5\frac{\gamma^4}{30\Gamma_3^2\Gamma_2^2}\left(\frac{\tau}{\tau_D}\right)^2\left[115\left(\frac{\tau}{\tau_D}\right)^2+126\gamma^2\left(\frac{\tau}{\tau_D}\right)+35\gamma^4\right]\right\}.
\end{aligned}
\tag{23}
$$

The intrinsic timescale of the CCF has to be related to a characteristic distance given by the separation of the two peaks δ of the twin-focal volume $\delta^2 = z_0^2 + \gamma^2\omega_\rho^2$. Indeed, $\tau_z/\tau_D = 1.24 + 0.31\,\gamma^2$ fits well for $\gamma > 2$, which is the typical case.

The relative contrast decreases for increasing longitudinal focus-spread as $G^{+-}_{\rm CCF}(\tau_z)/G_{\rm ACF}(0) \approx \left(17.4 + 8.27\gamma^2\right)^{-1}$. Since this expression is independent on the lateral focus-size ω_ρ, it may be used to estimate the beam-shape parameter γ.

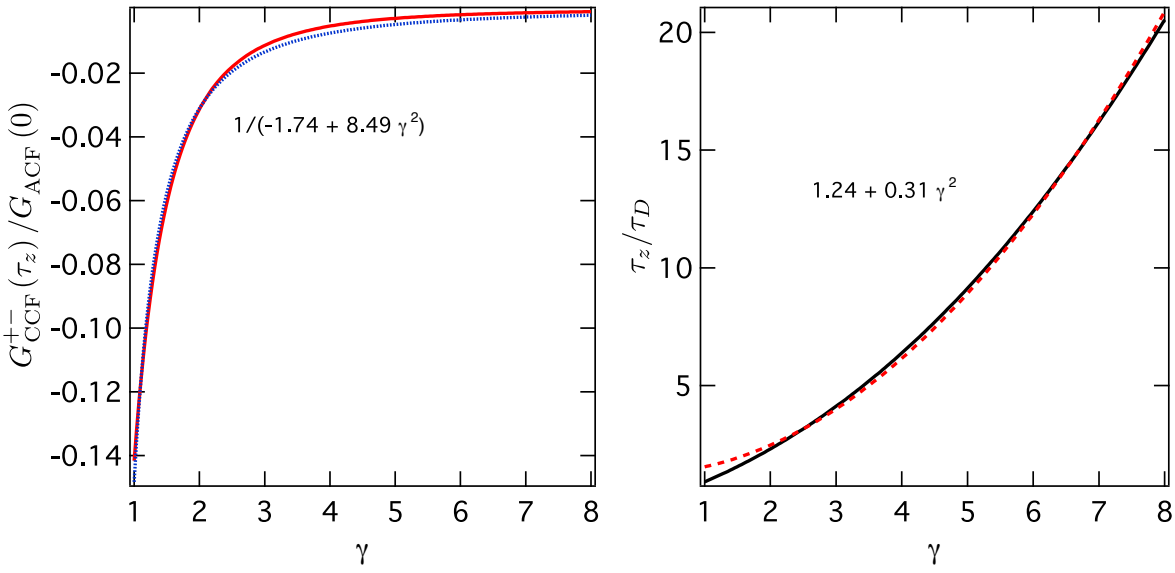

Figure 3: Contrast of the CCF and the characteristic cross-correlation time.

2.7 Absolute value auto-correlation functions, $G^{\mathrm{abs}}_{\mathrm{ACF}}$

The auto-correlation function of the absolute value of the photothermal signal may be computed numerically only in case of flow or asymmetry. We find

$$G^{\mathrm{abs},V_z,z_0}_{\mathrm{ACF}} = \frac{4\left(\frac{\tau}{\tau_D}\right)^{1/2}\exp\left(2Z^2-\frac{V_z^2\tau^2}{\omega_\rho^2}\frac{\tau_D}{\tau}\right)}{\langle C\rangle\pi^{3/2}\gamma^2\,\omega_\rho^5\,\Gamma_1\Gamma_3\left[1+\sqrt{\pi}Z\exp\left(Z^2\right)\mathrm{Erf}(Z)\right]^2}\left[\int_{-\infty}^{\infty}\mathrm{d}z'\exp\left(-az'^2\right)\right.$$
$$\left.\times\exp\left(z_0\left[bz'-f-az_0\right]\right)\exp\left(fz'\right)|z'-z_0|\left\{1+\exp\left(K^2\right)K\sqrt{\pi}\,\mathrm{Erf}(K)\right\}\right], \tag{24}$$

$$G^{\mathrm{abs},V_z}_{\mathrm{ACF}} = \frac{4\left(\frac{\tau}{\tau_D}\right)^{1/2}\exp\left(-\frac{V_z^2\tau^2}{\omega_\rho^2}\frac{\tau_D}{\tau}\right)}{\langle C\rangle\pi^{3/2}\gamma^2\,\omega_\rho^5\,\Gamma_1\Gamma_3}\int_{-\infty}^{\infty}\mathrm{d}z'\exp\left(-az'^2+fz'\right)|z'|\left\{1+\exp\left(H^2\right)H\sqrt{\pi}\,\mathrm{Erf}(H)\right\}, \tag{25}$$

$$G^{\mathrm{abs}}_{\mathrm{ACF}} = \frac{\frac{\gamma^2}{2}\left[\frac{\pi}{2}-\arctan\left(\frac{2}{\gamma^2}\sqrt{\frac{\tau}{\tau_D}\Gamma_2}\right)\right]+\sqrt{\frac{\tau}{\tau_D}\Gamma_2}}{\langle C\rangle\,\pi^{3/2}\Gamma_1\Gamma_2^{3/2}\omega_\rho^3}. \tag{26}$$

where Eqns. 25 and 26 are special cases of Eqn. 24. Indeed, the statement that $G_{\mathrm{ACF}}(\tau)-G^{\mathrm{abs}}_{\mathrm{ACF}}(\tau)=4G^{+-}_{\mathrm{CCF}}(\tau)$ holds true, which was a claim of the paper, can be seen.

For *small axial flow velocities* the absolute value ACF reads:

$$G^{\mathrm{abs},V_z}_{\mathrm{ACF}} \approx \exp\left(\frac{-V_z^2\tau_D^2}{\omega_\rho^2}\frac{\tau}{\tau_D}\right)\left[G^{\mathrm{Abs}}_{\mathrm{ACF}}+\left(\frac{V_z\tau_D}{\omega_\rho}\right)^2 2\gamma^3\left(\frac{\tau}{\tau_D}\right)\frac{2\left(\frac{\tau}{\tau_D}\right)^{1/2}\left(4\frac{\tau}{\tau_D}+\gamma^2\right)\Gamma_2^{1/2}+\left[\gamma^4-4\left(\frac{\tau}{\tau_D}\right)^2\right]\left[\frac{\pi}{2}-\arctan\left(\frac{2}{\gamma^2}\sqrt{\frac{\tau}{\tau_D}\Gamma_2}\right)\right]}{\pi\Gamma_3\Gamma_1\Gamma_2^{5/2}}\right], \tag{27}$$

which, as for the phase-sensitive ACF Eqn. 15, shows a quadratic dependence on the flow-velocity V_z.

2.8 Single lobe auto-correlation functions, G^{+}_{ACF}

The following ACFs use the correct self-normalization as mentioned in the data processing section. For the symmetric configuration this means a normalization by $\left(\int \Phi^{+}(\mathbf{r})\,\mathrm{d}\mathbf{r}\right)^2 = \left(\frac{\pi}{8}\omega_z^2\omega_\rho^2\right)^2$.

$$G^{+,V_z,z_0}_{\mathrm{ACF}} = \frac{8\left(\frac{\tau}{\tau_D}\right)^{1/2}\exp\left(2Z^2-\frac{V_z^2\tau^2}{\omega_\rho^2}\frac{\tau_D}{\tau}\right)}{\langle C\rangle\pi^{3/2}\gamma^2\,\omega_\rho^5\,\Gamma_1\Gamma_3\left\{1+\sqrt{\pi}Z\exp\left(Z^2\right)[1+\mathrm{Erf}(Z)]\right\}^2}\left[\int_{-\infty}^{z_0}\mathrm{d}z'\exp\left(-az'^2\right)\right.$$
$$\left.\times\exp\left(z_0\left[bz'-f-az_0\right]\right)\exp\left(fz'\right)\left[z_0-z'\right]\left\{1-\exp\left(K^2\right)K\sqrt{\pi}\left[1-\mathrm{Erf}(K)\right]\right\}\right], \tag{28}$$

$$G^{+,V_z}_{\mathrm{ACF}} = \frac{-8\left(\frac{\tau}{\tau_D}\right)^{1/2}\exp\left(-\frac{V_z^2\tau^2}{\omega_\rho^2}\frac{\tau_D}{\tau}\right)}{\langle C\rangle\pi^{3/2}\gamma^2\,\omega_\rho^5\,\Gamma_1\Gamma_3}\int_{-\infty}^{0}\mathrm{d}z'\exp\left(-az'^2+fz'\right)z'\left\{1-\exp\left(H^2\right)H\sqrt{\pi}\left[1-\mathrm{Erf}(H)\right]\right\}, \tag{29}$$

$$G^{+}_{\mathrm{ACF}} = \frac{\frac{\gamma^2}{2}\left[\pi-\arctan\left(\frac{2}{\gamma^2}\sqrt{\frac{\tau}{\tau_D}\Gamma_2}\right)\right]+\sqrt{\frac{\tau}{\tau_D}\Gamma_2}}{\langle C\rangle\pi^{3/2}\omega_\rho^3\,\Gamma_1\Gamma_2^{3/2}}, \tag{30}$$

where Eqns. 29 and 30 are special cases of Eqn. 28. The contrast for the symmetric cases ($z_0 = 0$) is given by $G^{+,V_z}_{\mathrm{ACF}}(0) = G^{+}_{\mathrm{ACF}}(0) = 1/\langle N\rangle$ with $\langle N\rangle = \langle C\rangle V_{\mathrm{eff}}$. Here, the effective volume is half that of the symmetric dual lobe focal volume: $V_{\mathrm{eff}} = 2\sqrt{\pi}\gamma\,\omega_\rho^3$. The negative lobe ACF, G^{-}_{ACF}, is connected by symmetry to the above expression via $G^{-,V_z,z_0}_{\mathrm{ACF}} = G^{+,V_z,-z_0}_{\mathrm{ACF}}$.

2.9 Note on the implemenation of the CFs

Notice that $|H|$ and H^2 get very large for small $\tau \ll \tau_D$ and moderate z such that $z/\tau \gg V_z$:

$$H = \frac{bz-f}{2\sqrt{a}} = \frac{\left[\left(\frac{\tau_D}{\tau}\right)z - V_z\tau_D\right]\frac{1}{\omega_\rho}}{\sqrt{\left(\frac{\tau_D}{\tau}\right)+\frac{2}{\gamma^2}}} \to \frac{z}{\omega_\rho}\sqrt{\frac{\tau_D}{\tau}} \tag{31}$$

Thereby, the term $\exp(H^2) \to \pm\infty$ becomes non-computable for regular programs for small lag-times. However, $az^2 \to \frac{z^2}{\omega_\rho^2}\left(\frac{\tau_D}{\tau}\right)$ grows large in the same way. Thus, to circumvent the numerical problem, the term $\exp(-az'^2)\exp(H^2)$ should be written as $\exp(H^2-az'^2)$ and the argument be computed first.

2.10 Considering twin focus with two different beam-waists

If two distinct lobe-widths are assumed, which can be a direct consequence of the in-plane asymmetry of the tightly focused laser-beam fields if they display strong aberration, and we set $\omega_{\rho,-} = g\,\omega_{\rho,+}$ and still use $\tau_D = \omega_{\rho,+}/(4D)$ we find

$$\frac{(4\pi D\tau)^{-3/2}}{\langle C\rangle}\int_{\phi,\phi'=0}^{2\pi}\int_{\rho,\rho'=0}^{\infty}\Phi_\rho\,\mathrm{d}\phi\,\mathrm{d}\phi'\rho\,\mathrm{d}\rho\,\rho'\mathrm{d}\rho'\left[1-\Theta(z)\right]\Theta\left(z'\right)\exp\left(-\frac{2\rho^2}{\omega_{\rho,+}}-\frac{2\rho'^2}{\omega_{\rho,-}^2}\right) = \frac{\omega_{\rho,+}\pi^{1/2}g^2}{4\langle C\rangle\left(\frac{1+g^2}{2}+\frac{\tau}{\tau_D}\right)\left(\frac{\tau}{\tau_D}\right)^{1/2}} \tag{32}$$

and we find instead the following normalization: $\left[\pi\,\omega_z^2\,\omega_{\rho,+}^2\left(1+g^2\right)/8\right]^2$. This result, however, may be used in the case of the evaluation of the cross-correlation function only and was not used in the analysis presented in the paper.

3 Radiation Pressure

3.1 Radiation pressure forces

The axial force within the generalized Lorenz-Mie theory (GLMT) is given by $c\,F_z = n_m\,I_0\,\sigma_{\mathrm{pr},z}$, where $\sigma_{\mathrm{pr},z}$ is the radiation pressure cross-section (given in detail in ref. [**?**, **?**]), c is the speed of light and $I_0 = 2P_0/\pi\omega_0^2$ is the focus intensity of the Gaussian beam. In case of a small particle, i.e. small size parameter $x = 2\pi n_m R/\lambda \ll 1$, and large skin-depth $\delta_s \gg R$ as compared to the particle size (where $\delta_s^{-2} = k^2\,\mathrm{Im}\sqrt{\epsilon_p}$ holds, and ϵ_p is the complex permittivity of the particle), the

Rayleigh-Approximation (RA) permits the evaluation of the radiation forces via

$$\textbf{total force:} \quad \mathbf{F}_{\rm rad} = F^{\rm abs}_{\rm rad}\hat{\mathbf{e}}_z + F^{\rm sca}_{\rm rad}\hat{\mathbf{e}}_z + \mathbf{F}^{\rm grad}_{\rm rad}, \tag{33}$$

$$\text{absorption force:} \quad F^{\rm abs}_{\rm rad} = \frac{n_m}{c} I(\mathbf{r})\sigma^{\rm pw}_{\rm abs} \quad \text{with} \quad \sigma^{\rm pw}_{\rm abs} = -k\,{\rm Im}(\alpha), \tag{34}$$

$$\text{scattering force:} \quad F^{\rm sca}_{\rm rad} = \frac{n_m}{c} I(\mathbf{r})\sigma^{\rm pw}_{\rm sca} \quad \text{with} \quad \sigma^{\rm pw}_{\rm sca} = k^4|\alpha|^2/6\pi, \tag{35}$$

$$\text{gradient force:} \quad \mathbf{F}^{\rm grad}_{\rm rad} = \frac{n_m}{2c}|\alpha|\nabla I(\mathbf{r}), \tag{36}$$

with $\sigma^{\rm pw}_{\rm abs}$ and $\sigma^{\rm pw}_{\rm sca}$ being the plane wave Rayleigh-regime absorption and scattering cross-sections expressed as a function of the complex polarizability α of the particle of permittivity $\epsilon_n = \sqrt{n_m}$ and effective volume V, $\alpha = 3V\left(\epsilon_p - \epsilon_m\right)/\left(\epsilon_p + 2\epsilon_m\right)$. Also, $k = 2\pi n_m/\lambda$ is the wave-number in the medium. The deviation of the RA with regard to the GLMT calculation as observed in table 3 is expected since the skin-depth of Gold at this wavelength, $\delta_s = 38\,$nm, is comparable to the particle dimensions used here. As a calculation check, the forces and absorption cross-section for a very small particle ($R = 5$ nm) has been added where both theories agree. Between the absorption cross-sections for the heating laser beam wavelength and the detection beam wavelength a factor 24 and 18 are found for $R = 14$nm and $R = 30$nm, respectively.

Table 3: Axial Radiation Pressures at $z = 0$ on AuNPs, $n_m = 1.33$, $P = 1.0$ mW.

Wavelength λ [nm]	ω_0 [nm]	Radius R [nm]	F_z (GLMT / RA)	$\sigma_{\rm abs}$ [m^2] (GLMT / RA)
532	215	14	59 fN / 62 fN	7.5×10^{-16} / 9.9×10^{-16}
532	215	30	733 fN / 757 fN	7.6×10^{-15} / 7.8×10^{-15}
635	266	14	1.7 fN / 1.8 fN	3.1×10^{-17} / 4.0×10^{-17}
635	266	30	44 fN / 35 fN	4.1×10^{-16} / 4.0×10^{-16}
635	10^4	5	5.28×10^{-20} N / 5.22×10^{-20} N	1.86×10^{-18} / 1.84×10^{-18}

3.2 Hot Brownian motion and drag

The following parameters for water were used to get the curve in Fig. 4 b) [**?**, **?**]: Thermal conductivity $\kappa = 0.63\,{\rm Wm^{-1}K^{-1}}$, viscosity $\eta(T) = \eta_\infty \exp(A/(T - T_{\rm VF}))$, $T_{\rm VF} = 152$K, $A = 497$, $\eta_\infty = 2.98\times10^{-5}\,{\rm Nsm^{-2}}$. The beam shape parameters were obtained using the GLMT framework as explained in detail in [**?**]. After the calibration with immobilized AuNPs in a PDMS matrix the only parameters changed were ${\rm NA_{ill}} = 1.33$ to account for the total internal reflection at the water-glass interface and $n_2 = 1.33$ as well as ${\rm d}n/{\rm d}T = 2.2\times10^{-4}\,{\rm K^{-1}}$ to change from PDMS to water. A focal depth of $d = 15\mu$m was taken as in the experiment. This immediately gives $\sigma^E_{\rm ill} = 3.99\times10^{-6}{\rm m^2}$, $\sigma^E_{{\rm abs},h} = 1.1\times10^{-7}{\rm m^2}$, $\sigma^E_{{\rm abs},d} = 3.7\times10^{-9}{\rm m^2}$ and the beam shape parameters $\gamma = 3.65$ and $\omega_\rho = 197\,$nm.

$$\Delta T = c_{T,\lambda}\frac{\sigma^E_{\rm abs}}{\sigma^E_{\rm ill}}\frac{P_{{\rm inc},h}}{4\pi\kappa R} \tag{37}$$

with these values we obtained, using $k_B = 1.38\times10^{-23}\,{\rm J/K}$ and $R = 30\,$nm and $\theta = \Delta T/(T_0 - T_{\rm VF})$

$$\Delta T_{\rm HBM} \approx T_0 + \frac{1}{2}\frac{\Delta T}{T_0} + \left[\ln\frac{\eta_0}{\eta_\infty} - 1\right]\frac{\Delta T^2}{12T_0^2} + \mathcal{O}\left(\frac{\Delta T^3}{T_0^3}\right) \tag{38}$$

$$\frac{\eta_0}{\eta_{\rm HBM}} \approx 1 + \frac{193}{486}\left[\ln\frac{\eta_0}{\eta_\infty}\right]\theta - \left[\frac{56}{243}\ln\frac{\eta_0}{\eta_\infty} - \frac{12563}{118098}\ln^2\frac{\eta_0}{\eta_\infty}\right]\theta^2 + \mathcal{O}\left(\theta^3\right) \tag{39}$$

$$D_{\rm HBM} = \frac{k_B T_{\rm HBM}}{6\pi\eta_{\rm HBM}R} \tag{40}$$

$$\tau_{D,{\rm HBM}} = \frac{\omega_\rho^2}{4D_{\rm HBM}} = \frac{3\pi\eta_{\rm HBM}R\,\omega_\rho^2}{2k_B T_{\rm HBM}} \tag{41}$$

3.3 Radiation pressure induced flow

The axial flow velocity in the ADE will follow the spatial intensity pattern of the heating laser.

$$\mathbf{V}(\mathbf{r}) = \frac{\mathbf{F}_{\mathrm{rad}}(\mathbf{r})}{6\pi\eta_{\mathrm{HBM}}(\Delta T(\mathbf{r}))R} \tag{42}$$

Since it is primarily the heating-laser which transfers its energy and thus also its momentum to the particle, the flow induced will primarily be axial and heating laser induced. Therefore, the simplifying assumption of a constant (effective, see definition of ζ in the next section) axial flow was used in the discussion in the main article:

$$\mathbf{V}(\mathbf{r}) \quad \equiv \quad \zeta\mathbf{V} \quad \approx \quad \zeta\frac{F_{z,\mathrm{rad}}(z=0)}{6\pi\eta_{\mathrm{HBM}}R}\hat{\mathbf{z}} \tag{43}$$

3.4 Effective parameters for Gaussian heating and pushing

Since the radiation-pressure induced axial flow velocity $\mathbf{V} = V_z\hat{\mathbf{z}}$ and the induced temperature ΔT are non-uniform in space when a focused laser beam is used, an effective value which is smaller than the peak value for both effects obtained in the focus is expected to be extracted from the data when analyzed with the correlations function with constant V_z. If the resonant heating laser beam focused in the coordinate origin is assumed to be the major contribution, this means that $V_z^{\mathrm{eff}} = \zeta V_{z,0}$ and $\Delta T^{\mathrm{eff}} = \zeta\Delta T$ with some $\zeta < 1$ and where $V_{z,0}$ and ΔT are the values for the induced flow velocity and the temperature-increment when the particle is in the focus. A 3D-Gaussian profile may be used to estimate the value of ζ via

$$\zeta \approx \frac{\int V_z(\mathbf{r})\times I(\mathbf{r})\,\mathrm{d}\mathbf{r}}{\int I(\mathbf{r})\,\mathrm{d}\mathbf{r}}/V_{z,0} = \frac{\int_0^\infty \mathrm{d}\rho\int_0^{2\pi}\mathrm{d}\phi\int_{-\infty}^{\infty}\mathrm{d}z\left[\exp\left(-\frac{2\rho^2}{\omega_\rho}\right)\exp\left(-\frac{2z^2}{\omega_z}\right)\right]^2}{\int_0^\infty \mathrm{d}\rho\int_0^{2\pi}\mathrm{d}\phi\int_{-\infty}^{\infty}\mathrm{d}z\exp\left(-\frac{2\rho^2}{\omega_\rho}\right)\exp\left(-\frac{2z^2}{\omega_z}\right)} = \frac{1}{2\sqrt{2}} \approx 0.35 \tag{44}$$

4 Twin-PhoCS in living Cells

Photothermal measurements have been carried out in MCF-10A cells. For topographical orientation the scattering signal of the detection laser was recorded as well. The images are taken by raster scanning the whole sample. AuNP were prepared according to [**?**] and mixed to the cell medium. The cells were incubated for 4 h with this AuNP-rich medium. The left column of figure 4 shows the scattering images of a cell that are superimposed with the photothermal signal of the AuNPs (red). In the surrounding medium red lines or single red pixels are dominant that corresponds to AuNP diffusing through the detection volume while scanning the sample. In the cell fixed AuNP can be detected (red circles). The right column of figure 4 shows z-scans through the sample. The green line marks the border between cell and the surrounding medium. The twin-focus of the photothermal can be identified for fixed AuNPs even in the cell volume. The bottom graph shows two axial line scans through the position of a AuNP at the glass interface (red) and in the cell (black).

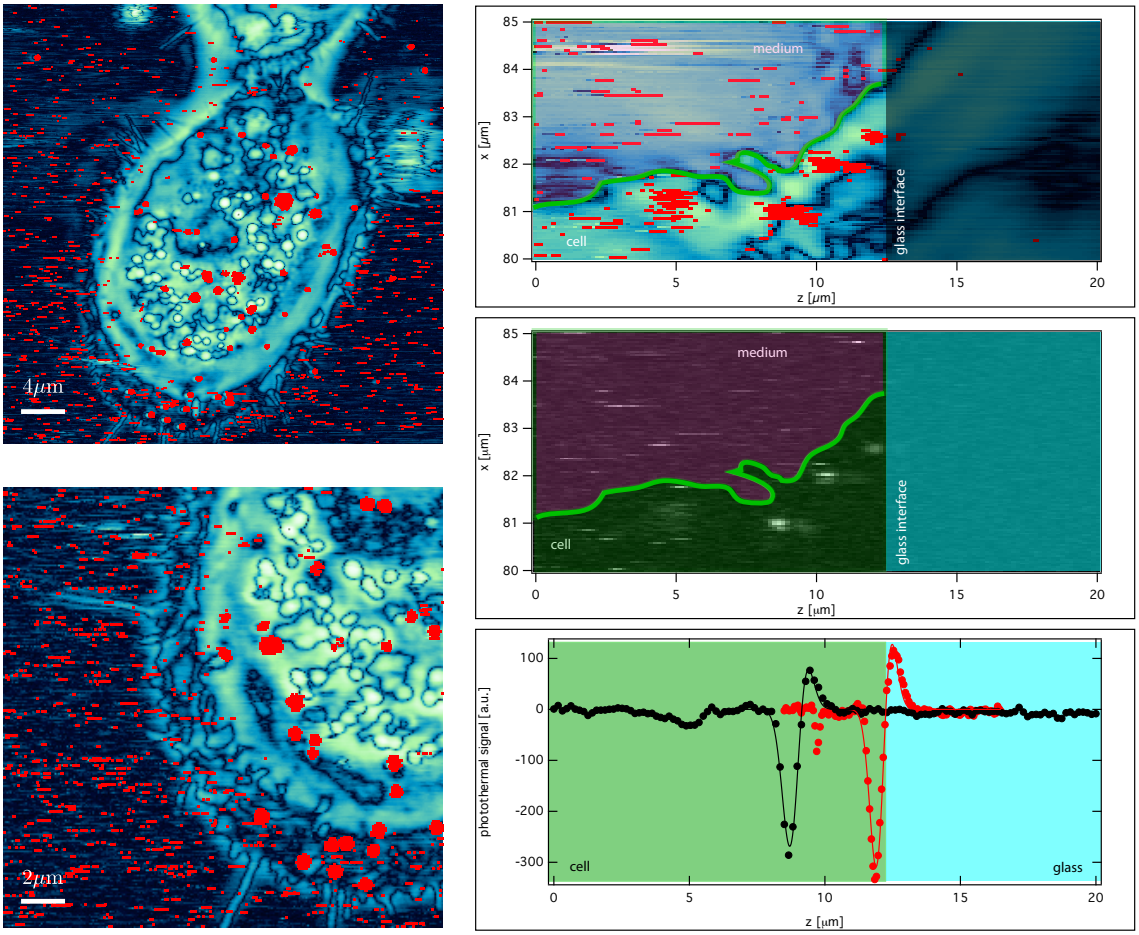

Figure 4: (left) Scattering images of a MCF-10A cell superimposed with the pt signal of diffusing AuNPs in the medium (red lines) and of bound AuNPs in the cell (filled red circles). (right) zx-scans of the scattering and the pt signal (top), pt (middle), line scan through a fixed AuNP on the glass surface (bottom red) and through a AuNP in the cell (bottom, black).